Kinetic Study on the Hydrogen Reduction of Some Nonferrous Metal Oxides

By

Akio YAMAGUCHI* and Jyoichiro MORIYAMA*

(Received June 30, 1966)

To investigate the kinetic aspects in reactions involving solids, the reduction rate of nickel oxide by hydrogen was measured by means of thermo-balance. The rate is described by 2/3 order kinetic law and has an activation energy of 25 kcal/mol.. From the results of Delmon's interruption technique and other kinetic examination, it may be assumed that the reduction will proceed according to the spherical surface contracting model. The reduction rate of several ilmenite ores was also measured by the same means and the profiles of oxygen concentration in a section of reduced particles were examined by means of X-ray micro-analyser to inspect the reduction progress. It was found that the reduction process consists of two stages proceeding successively, where in the first stage, the reduction of iron oxide besides ilmenite component occurred, secondly, the latter component was reduced and those kinetics were also described approximately by 2/3 order law.

1. Introduction

The heterogeneous reactions between gases and solids utilized for many industrial processes of metallurgy have been widely studied. Although the thermodynamical properties and equillibrium diagrams are known, there are numerous problems still unsolved in the fields of kinetics and mechanisms in those reactions.

Thus, the reduction of non-ferrous metal oxides is selected as the typical example to study the following reaction formula,

$$(\mathrm{Solid})_1+(\mathrm{Gas})_1 \rightleftarrows (\mathrm{Solid})_2+(\mathrm{Gas})_2$$

and as parts of the investigation pertaining to the above-mentioned subjects, first, the reduction of nickel oxide with hydrogen that has been studied by many investigators was undertaken to affirm the kinetic aspects experimentally. The applicability of the above kinetic schema to hydrogen reduction of several ilmenite ore was examined by means of an X-ray and X-ray probe micro-analyser. From the above results the possible mechanism in latter reduction was discussed.

* Department of Metallurgy.

2. The description of Rate Equation

Graphs of extent of reduction x as a function of time t for such reductions have generally characteristic sigmoid shapes, which are almost the same as the ones for the thermal decomposition of inorganic compounds. These phenomena have been also observed in the studies of hydrogen reduction of nickel oxide[1~4], ferric oxide[5] and cupurric oxide[6] and the like, and may be interpreted as follows: some nuclei are produced at a localized place on the surface of particles, these nuclei grow, and beyond the point of inflexion, the reaction decays as nuclei overlap and the area of interface between metal oxide and the metal phase decreases.

According to this concept, K. Mampel[7] has discussed the heterogeneous reaction and deduced some equation. Lately, B. Delmon[8] has summarized a further extensive mathematical and theoretical treatment of a random nucleation from which he has derived the same equation as Mampel's.

In the decaying period the reduction proceeds through a chemical process at the interface between the oxide/metal, and its kinetic equation is expressed by

$$\frac{dx}{dt} = k(1-x)^{2/3} \qquad (1)^*$$

where k^* is rate constant. Eq(1) is derived by assuming that the shape of the oxide particle is spherical, the reduction proceeds from the outside surface towards the center and the rate is not controlled by diffusion but by chemical reaction together with the advance of interface as above-mentioned, and therefore the rate will be directly proportional to the area of interface. Integrating Eq (1), we have

$$1-(1-x)^{1/3} = \frac{k}{r_0} = k't \qquad (2)^*$$

where k and k' are rate constants and r_0 is the radius of a particle.

The assumption described above which has been previously verified in the studies of Fe-oxide reduction[9], has been shown to be partially valid for the H_2 reduction of tungsten-trioxide by Authors[10].

In a case of ore such as ilmenite, however, it will be presumed that the reduction proceeds in an irregular manner because of the heterogeneity of the chemical composition, existence of impurities and the size-distribution of particles (Table 3). Rate equation (1) rewritten as a general form[11][12] on the assumption that the reduction rate is proportional to $1-n$ power of the unreduced fraction $(1-x)$, namely

---

* Rate constant is represented by k for convenience though each constant has a respective dimension.

$$\frac{dx}{dt} = -\frac{d(1-x)}{dt} = k(1-x)^{1-n} \qquad (3)^*$$

where $(1-n)$ is constant corresponding to a reaction order which is equal to 0.67 in equation (1). In the present works, the reduction rate of ilemnite was investigated by the application of equation (3).

3. Material

3.1 Preparation of nickel powder

Nickel nitrate (S.G reagent) was decomposed slowly at 450°C for 4 hrs and then treated at 900–920°C for 5 hrs after sieving under 200 mesh. The other nickel salts were prepared from 10% nickel nitrate solution preheated to 70–80°C to which a slight excess of 10% ammonium carbonate solution (for carbonate) or ammonia aq. (for basic hydroxide) was added. Then, the precipitate of nickel carbonate or hydroxide produced was filtered, washed completely and dried for one day. Each salt was decomposed in the same means of nickel nitrate. In the present work, each sample was prepared from carbonate, hydroxide and nitrate was indicated by the notation of CO–NiO, OH–NiO and NO•NiO respectively. From the results of specific surface area (BET: N_2 adsorption) and electromicroscopic examination, it may be assumed that the produced nickel oxide is not porous and the shape is nearly spherical.

3.2 ilmenite ore

The chemical analyses are shown in Table 1. According to the X-ray diffraction patterns, only $FeO \cdot TiO_2$ component could be detected, and others colud not.

Table 1. Chemical Compositions of each Ilmenite (wt %).

	$T \cdot TiO_2$	$T \cdot Fe$	FeO	Fe_2O_3	SiO_2	Al_2O_3	CaO
Ceylon	53.17	30.91	19.11	22.92	0.81	0.61	0.26
Australia	54.57	30.98	25.15	16.34	0.53	0.40	0.30
India	53.41	31.00	25.59	15.89	1.47	0.70	0.24
	MgO	Cr_2O_3	V_2O_5	MnO	P_2O_5	S	H_2O
Ceylon	0.92	0.09	0.19	0.94	0.05	0.03	0.18
Australia	0.32	0.04	0.13	1.67	0.06	0.01	0.13
India	1.32	0.07	0.18	0.39	0.06	0.01	0.11

4. Experimental Procedures and Results

The rate of reduction was determined by a thermobalance, and the cathetometer reading for weight loss was used as an indication of the extent of reduction.

The furnace temperatures were controlled by a potentiometrical thermostat with an accuracy of $\pm 1°C$.

Before commencing the experiment, the furnace temperature was adjusted to the desired one, while the sample was held in a basket and suspended by a quartz wire from a quartz spring balance in a vertical reactor. After the sample had attained the experimental temperature, the reactor was sealed and evacuated, and then the H_2 from a commercially avaiable bomb was introduced from the bottom after being passed through the purifier train. The flow rate of hydrogen and sample weight were affirmed in the preliminary experiments, as critical values which meant that the fluctuations would not affect the rate.

The other procedures and experimental conditions will be described when needed.

4.1 Reduction of nickel oxide

4.1.1 Reduction rate and kinetics—The results obtained on NO-NiO are shown in Fig. 1 as an example of the relation between the extent of reduction x and time t. Each of these reduction curves has a sigmoid type in shape and this fact is in good agreement with the one previously reported[1~4]:

The slope of a straight-line in the sigmoid curve and the intercept of tangent at time axis are denoted by k_e and t_i respectively. These two charactristic constants are plotted against the reciprocal temperature in Fig. 2. Apparent activation energy on k_e and t_i calculated according to Arrhenius relationship is

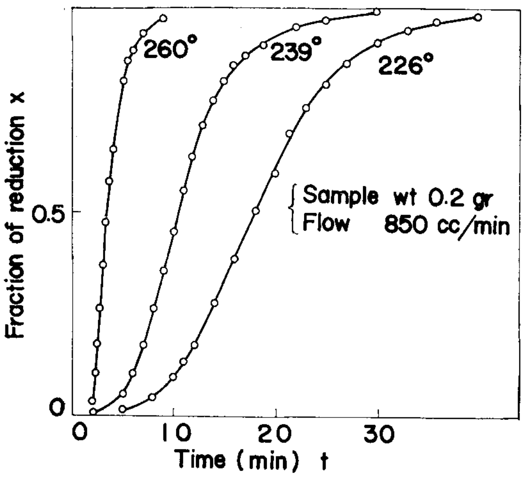

Fig. 1. Reduction curves of NiO at different temperatures.

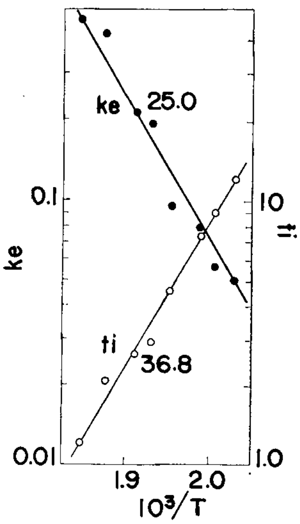

Fig. 2. Dependence of k_e, t_i on temperature.

25 kcal/mol. and −36.8 kcal/mol., respectively.

In Fig. 3, $1-(1-x)^{1/3}$ has been plotted against t in order to examine the results according to Eq. (2). These plots result in the straightline relation from 25–30 pct. up to 75 pct. reduction. Beyond 75 pct. reduction, however, deviation describing a parabolic law is obesrved. Temperature dependence of k is 25.6 kcal/mol.

Fig. 4 shows the changes of a specific surface area during reduction, where

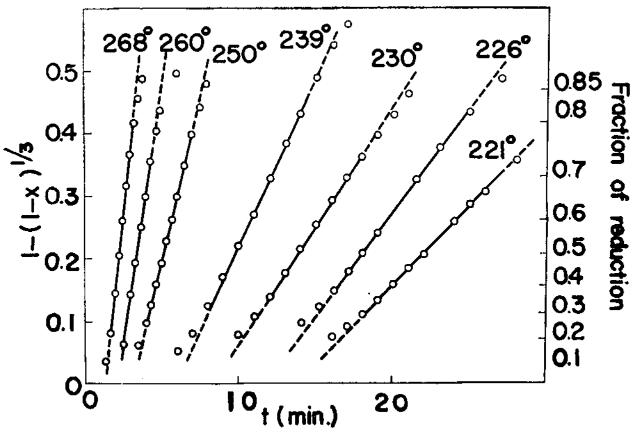

Fig. 3. Linear plots $1-(1-x)^{1/3}$ vs. time t, the rate equation of advance of interface $1-(1-x)^{1/3}=k_1t$.

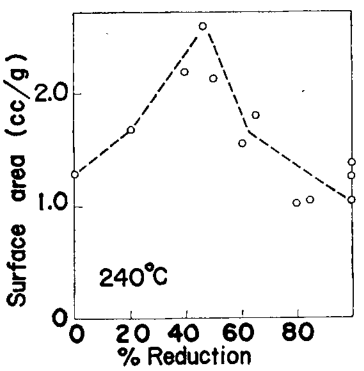

Fig. 4. Specific surface arrea changes by reduction.

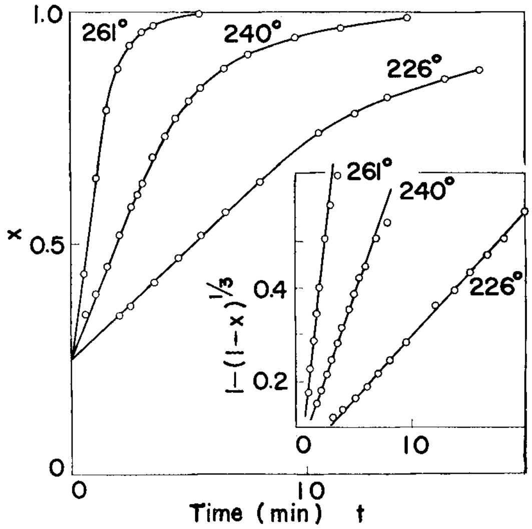

Fig. 5. Reduction curves, x vs. time and linear plots $1-(1-x)^{1/3}$ vs. t (pre-reduction 26%, 240°C)

the ordinate is indicated by the nitrogen gas adsorbed volume on cc/g calculated from B.E.T. isotherm. The increase of specific surface area up to 50 pct. reduction may be caused mainly by the formation of pore or the appearance of cracks and fissures. On the other hand, beyond 50 pct. reduction the surface area decreases gradually. This fact may be explained by the disappearance of fine pore or the change of crystal structure, but it will be more reasonable to consider that the mutual sintering between particles occurred, since it has been observed that the sample taken up after reduction to some extent was cohered as a whole. For this reason, reactional interface area decreases and resistance for diffusion of water vapor increases as reduction proceeds. Hence, its kinetics will be described by parabolic law.

Fig. 5 is an example of results obtained by Delmon's interruption technique[4)14)]. The plots of t against $1-(1-x)/^{1/3}$ are in a fairly good linear relation. The k by interruption one had a stronger dependence on temperature corresponding to the apparent activation energy of 31.5 kcal/mol. (see Fig. 8) and it was recognized that the rate varied depending on the temperature of inintial reduction.

4.1.2 Kinetic examination on Eq. (2)—The effect of particle size on the reduction rate at 260°C has been investigated using the crushed single crystals of various sizes with a weight of 25–30 mg and hydrogen flow of 200 cc/min. By plotting $\log 1-(1-x)^{1/3}$ against $\log t$, Fig. 6 is obtained. The abscissa is corrected to

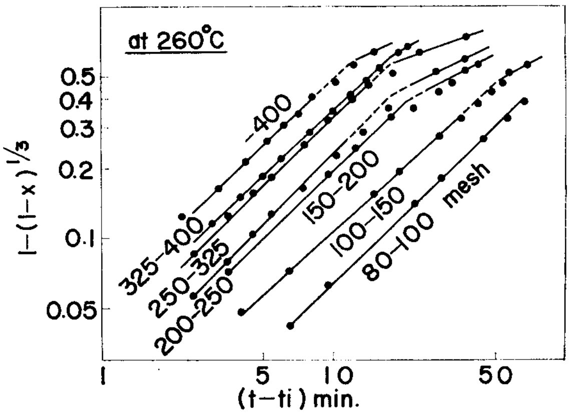

Fig. 6. Log-log plot according $1-(1-x)^{1/3}=kt$ for reduction of various particle size of crushed NiO single crystal.

$t-t_i$(t: the time elapsed in observation, t_i: the time elapsed in induction period). If Eq. (2) is valid, these plots sholud be a linear relation having a slope of unity. Those plots result in a group of parallel lines and as slope of the first-half line is close to unity which shows the approximation of Eq. (2). Further, Fig. 7 shows the effect of particle radii r on k. Theoretically, the plot of log k anainst log r should yield a straight line with a slope of negative unity as shown by the dotted line in Fig. 7. In the present case, since the samples should not be perfectly spherical but irregular in shape and properly contained particles which have some size distribution, it is difficult to expect that the relation resulting from Eq. (2) may be exactly in valid. However, those experimental data are placed dispersedly along the dotted line as is shown in Fig. 7, in other words, it will be more reasonable to consider that even if the particle below 325 mesh, under the present condition the reduction will proceed according to the process which is analogous to the mechanisms described by Delmon and others.

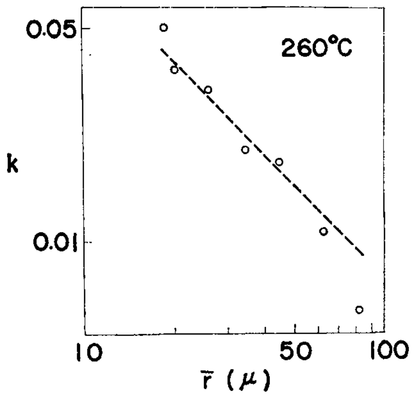

Fig. 7. Effect of particle size (mean value) on rate of reduction of single crystal.

4.1.3 Comparison of reduction rate among several nickel oxides.—Referring to the studies of hydrogen reduction of nickel oxide by Simnad[15] and Cech[2], it will be recognized that the early stage of reduction which includes the nucleation process starts from the defect points (containing cracks and fissures or the boundary of crystalline, etc.) situated dispresedly on the surface. Hence, the physical properties of surface and the variance of treatment which gives an influence on the surface property will presumably contribute to the variation of reduction rate. Each reduction rate of CO-NiO and OH-NiO at the temperature ranging from 230° to 270°C was measured by means of the Delmon's interruption technique with a sample weight of 40–50 mg and H_2 flow rate of 400 cc/min.

The k evaluated from Eq. (2) was plotted against the reciprocal of temperature (°K) as is shown in Fig. 8 with the data for NO-NiO in the previous test. From the above results, it can be found that the reduction rate becomes larger in the following order CO-NiO$<$OH-NiO$<$NO-NiO. The data for the activation energies is summarized in Table 2 with the other results.

By investigating the effect of particle size on k, for example at 230°C, the same relation of $k \propto r^{-1}$ as is shown in Fig. 7 is obtained. The result is shown in Fig. 9. The values of kr (μ/min, Table 2) reflecting the advance rate of interface at 230°C are in good agreement with each other except the single crystals. From

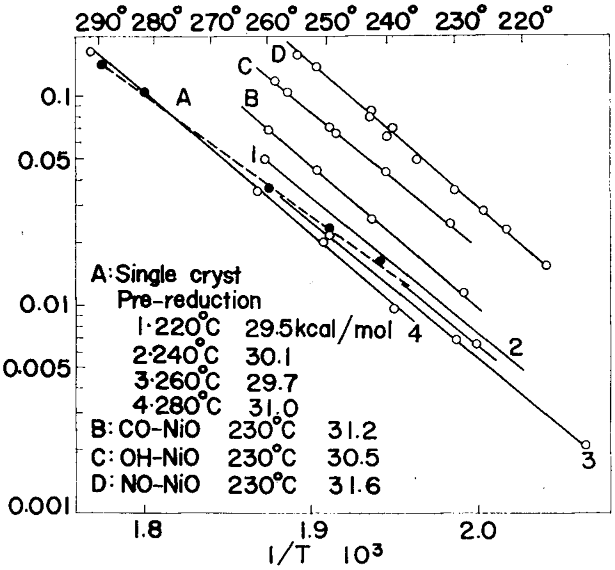

Fig. 8. Dependence of temperature on the reduction rate of various NiO powders.

Table 2. Activation energies and other data.

Material	Radius of particle (μ)	Activation energy (kcal/mol)	kr (μ/min, at 230°)
Single cryst.	20.5	30.0 (mean)	1.78×10^{-1}
CO-NiO	0.38	31.2	4.56×10^{-3}
OH-NiO	0.15	30.5	3.45×10^{-3}
NO_3-NiO	0.12	31.6	4.44×10^{-3}

the above results, it may be considered that the several nickel oxides prepared from their respective salt have only the effect of particle size on the rate and will have little difference in other properties.

4.2 Reduction of ilmenite ore

4.2.1 Rate and kinetic analysis—The reduction curves indicated no incubation period and no autocatalytic feature. The reduction starts at the maximum rate and then the rate decreases gradually.

It was found that the reduction rate increased as the ore size became smaller;

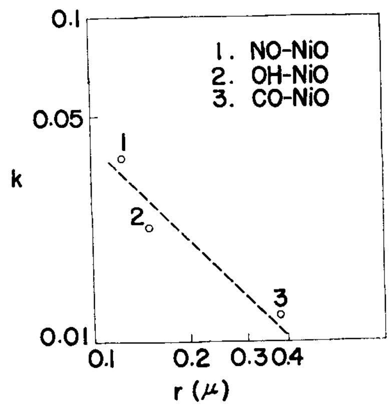

Fig. 9. The relation between rate const. k at 230°C and radius r of NiO particles prepared from various Ni-salts.

Table 3. Size distribution (wt %) of each ilmenite ore.

Mesh	80	80–100	100–150	150–200	–200
Australia	4.5	29.2	57.3	8.1	0.9
Ceylon	0	0.2	34.0	30.0	35.8
India	18.8	44.2	36.0	1.0	

that is, Ceylon ores had the largest rate and Indian the smallest (Table 3).

The reduction rate(r) was calcualted from the tangent of the curves. By plotting log r vs. $1/T$, the apparent activation energy was obtained, as is shown in Table 4. The first stage corresponds to the first half of the reduction curves, the second stage to the second half.

Table 4. Values of app. activation energy for H_2 reduction rate of each ilmenite.

	1st stage	2nd stage
Australia	21.3	34.4
Ceylon	22.0	32.1
India	21.8	28.8

From Eq. (3)

$$\log -\frac{d(1-x)}{dt} = \log k + (1-n) \log (1-x) \quad (4)$$

As can be seen from equation (4), $\log -d(1-x)/dt$ is the linear fucntion of $\log(1-x)$. The reaction order $(1-n)$ can be obtained from the slope of the straight line and also $\log k$ can be obtained from the intercept at the $\log -d(1-x)/dt$ axis.

The relation between $\log(-d(1-x)/dt)$ and $\log(1-x)$ for the reduction of Ceylon ilmenite ore was shown in Fig. 10 and those for Indian and Australizan were in similar fashion.

The mean reaction orders and the apparent activation energies on k are summarized in Table 5.

From the results of X-ray analyses, the diffraction line of metallic Fe and

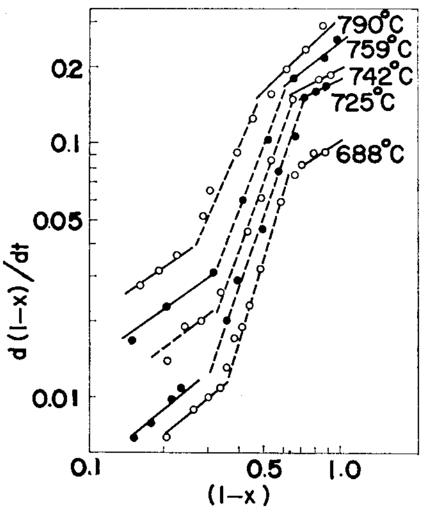

Fig. 10. $\log - d(1-x)/dt \sim \log (1-x)$ plots for Ceylon ores.

Table 5. App. activation energies and reaction order estimated for rate of each stage of ilmenite reduction by hydrogen.

	1st stage		2nd stage	
	order (1–n)	E (kcal/mol.)	order (1–n)	E (kcal/mol.)
Australia	0.89	20.4	0.77	27.0
India	0.87	19.5	0.68	29.0
Ceylon	0.78	20.8	0.72	28.3

TiO_2 (rutile) were confirmed and then became more intense, whereas that of $FeO \cdot TiO_2$ diminished gradually as the reduction proceeded.

Thus, since the X-ray analyses have not proved sufficiently, it was thought advisable to examine by means of X-ray micro-analyser for the above kinetic results.

4.2.2 Examination by X-ray microanalyses. (Table 6)—Photo (a)-(h) show X-ray characteristic image for each element in section of Australian ore particle reduced up to 70 pct. As shown in photo (d) (h), oxygen concentration has some gradients

Table 6. Condition of EMX analyses.

EMX	Shimazu ARL
Accelerating voltage	20 KV
Sample current	0.43 μA
Counter	flow proportional counter
Anal-crystal	A.D.P. (ammonium di-sulfate) for Ti LiF for Fe KAP (kalium acid) for O_2
Analyses	counting method by spot analysis
Counting time	30 sec.

in direction of raduii though the elements such as Ti, Fe and Mn are distributed homogeneously. The results of spot analyses by counting for oxygen concentration were shown in Fig. 11, 12, where the abscissa refers the position of anayses along the line of diameter and the ordinates are indicated by (R). Here, (R) is adopted as a fraction of unreduction for convenience because no avaiable data on correction of oxygen concentration by means of X-ray microanalyser. The values of (R) are calculated from the following equation.

$$(R)=\frac{(C, N \text{ in Sample})-(C, N \text{ in reduced ore})_m}{(C, N \text{ raw ore})_m-(C, N \text{ in reduced ore})_m}$$

C, N: Counting numbers for oxygen by spot analysis

$(C, N\cdots)_m$: mean value of C, N

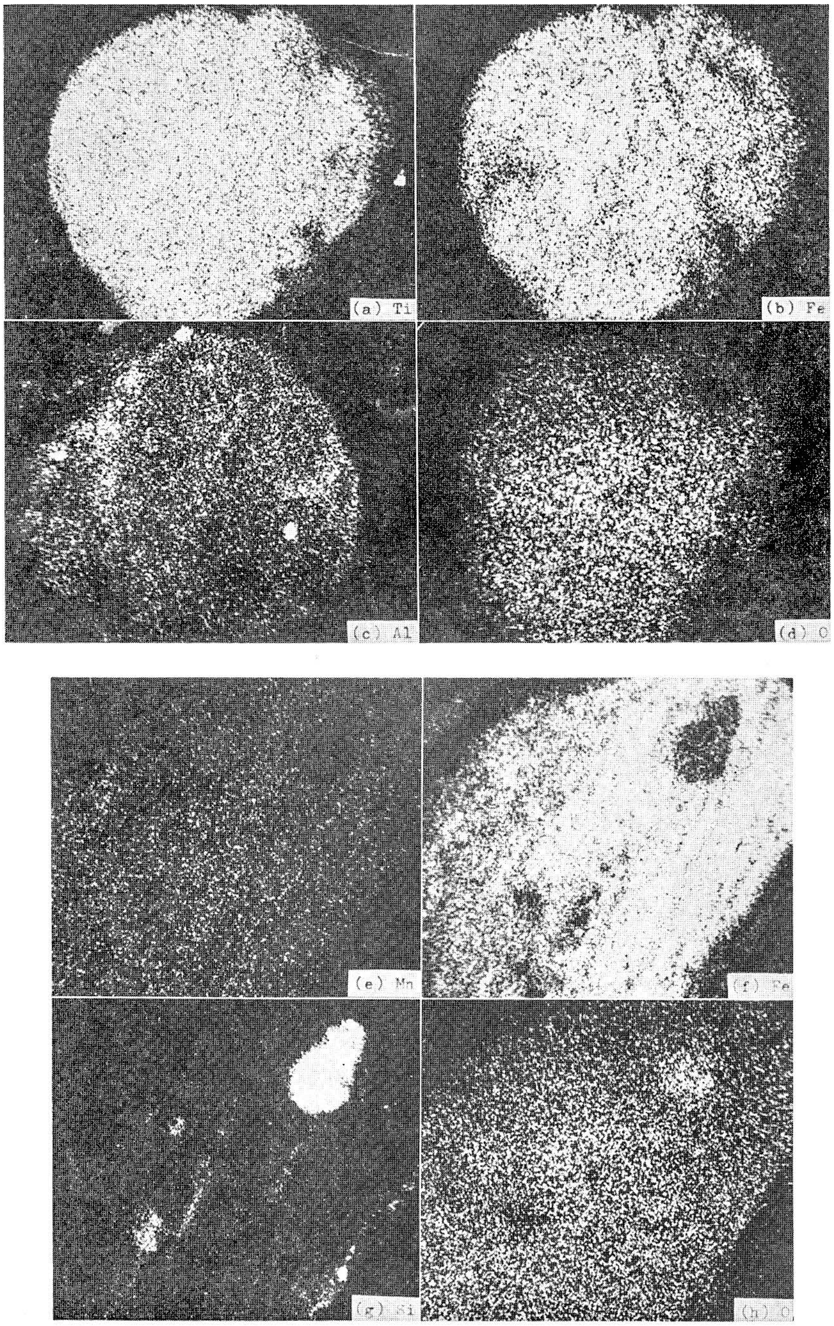

Photo. Characteristic X-ray image by
(a) Ti Kα (b) Fe Kα (c) Al Kα (d) O Kα
(e) Mn Kα (f) Fe Kα (g) Si Kα (h) O Kα

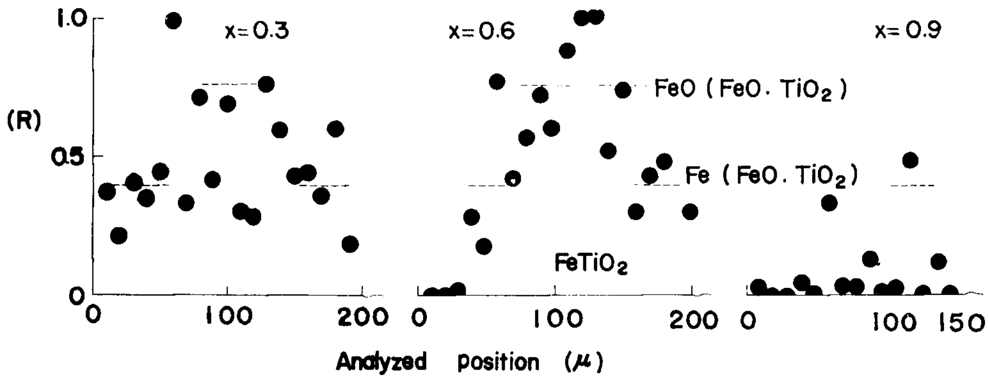

Fig. 11. Profile of oxygen concentration by spot analyses for Ceylon ilmenite ore.

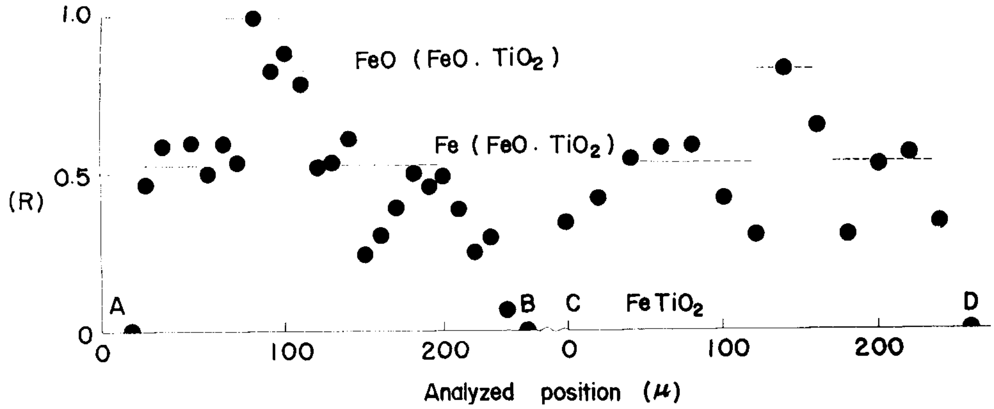

Fig. 12. Profile of oxygen concentration by spot analyses for Australian ore. ($x \sim 0.7$)

The profiles of oxygen concentration (Fig. 11, 12) are reflected in the situation of X-ray characteristic image for oxygen (photo d, h). From these facts it is supposed that the reduction started at the surface and proceeded into the interior.

Hussein[16] has found that in the Egyptian ilmenite iron oxides, ilmenite and

Table 7. Possible phase layer in reduced ilmenite ore and corresponding value of (R).

	(R)	
Possible phase	Australia	Ceylon
Fe_2O_3 ($FeO \cdot TiO_2$)	100	100
Fe_3O_4 ($FeO \cdot TiO_2$)	94.8	93
FeO ($FeO \cdot TiO_2$)	84.4	79.4
Fe ($FeO \cdot TiO_2$)	53.3	38.2
$Fe \cdot TiO_2$	0	0

rutile were reduced successively by hydrogen as the temperature increased. Supposing the reduction proceeds on order as above-mentioned, (R) calculated from the chemical analysis (Table 1) and possible phases resulting in reduction were summarized in Table 7.

5. Discussion

5.1 Kinetic examination

Since the reduction rate for principal period of nickel oxide prepared from various materials could be nearly described by Eq. (1), it seems reasonable to assume that the reduction nearly proceeds according to the mechanism analogous to centripetal progress of interface, and therefore, the data of activation energies seem to reflect the chemical process at interface regarded as the rate controlling factor.

However, when the fine particles are used as sample, it is difficult to suppose that the reactional interface can be exactly expressed by the extent of reduction. Also, the reduction will be disturbed by the water vapor as a product and especially beyond 50 pct. the reduction from the surface of assemblage of fine powder to interior will simultaneously proceed in addition to the reduction in each particle. From the above consideration, it seemed that the assumption for Eq. (1) or (2) is difficult to be valid strictly and consequently may be applicable only with approximation. In this meaning, the k becomes a mean value. However, the value may be used as the representative one for the rate of reduction depending upon the temperature and other kinetic parameters.

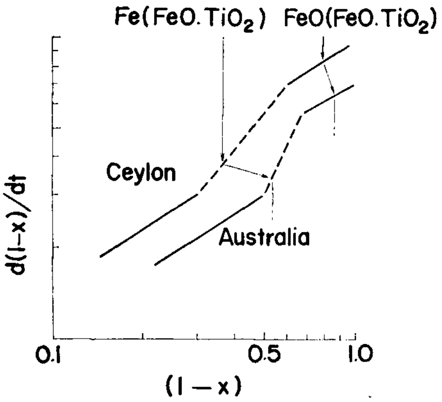

Fig. 13. Typical diagram of $\log \frac{d(1-x)}{dt} \sim \log(1-x)$ plot for reduction of Ceylon and Australian ilmenite ore by H_2

The reaction order on reduction of ilmenites is more or less larger than that of Eq. (1). S.J. Teichner et al[12] have pointed out that this order increases as standard deviation in normal size distribution increases. Therefore, it may be considered that the above facts will be due to the polydisperse of particle size in addition to heterogeneity of impurities, and considering size dependence of rate, (Fig. 13) the reduction proceeds nearly analogous to the case of nickel oxides.

5.2 Reduction mechanism of ilmenties

Typical plots according to Eq. (4) for the reduction of Ceylon and Australian ore were shown in Fig. 13 where the extent of first stage of Ceylon is larger and the one of second stage is shorter than Australian. This situation on the first stage is equivalent to Fe^{3+} content in ilmenite ores (Table 1). On the other hand, $\alpha-Fe$ could be detected by means of X-ray analysis before the reduction reached to 15 pct., while, as shown in Fig. 11, no points corresponding to $(R)=0$ were present. These facts suggest that iron oxides besides ilmenite component will be reduced during the first stage. Further, from the consideration of reaction kinetics, reduction during the first stage proceeds as follows,

$$Fe_2O_3\,(FeO\cdot TiO_2) \longrightarrow Fe_3O_4\,(FeO\cdot TiO_2) \longrightarrow$$
$$FeO\,(FeO\cdot TiO_2) \longrightarrow Fe\,(FeO\cdot TiO_2)$$

Consequently, on the basis of discussion mentioned above, it may be concluded that ilmenite component will be reduced during second stage as follows:

$$Fe\,(FeO\cdot TiO_2) \longrightarrow Fe\cdot TiO_2$$

Fig. 14 drawn on the basis of Fig. 11 illustrates the above-mentioned reduction processes of ilmenite ore.

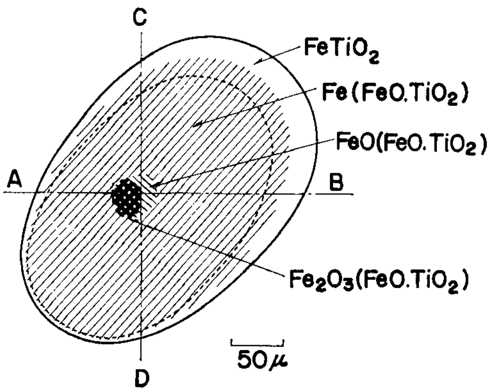

Fig. 14. Multiple-layer structure in partly reduced ilmenite ore. ($x\approx0.7$)

That the kinetic consist of two stage can be illustrated supposing that the interfacial reduction controlling the rate is different from each other and each stage has a respective apparent activation energy. From the fact that the apparent activation energy in the reduction of ilmenite is larger than that in the reduction of iron oxides[9)17)18)], it may be considered that the iron oxide in ilmenite ore is associated physically or chemically with the titanium oxide and the latter plays a role of negative induced reduction.

Summary

1) In studies on the hydrogen reduction of nickel oxide, it has been confirmed that the reduction rate were described approximately according to the sphere surface contracting model, the rate constants were inversely proportional to the

particle radii, and from the results by Delmon's interruption technique, the rate was affected by the initial condition of reaction and further, the apparent activation energies with 29.0–31.6 kcal/mol. have scarcely varied by the species of samples.
2) From the above-mentioned results, it seems reasonable to assume that when the experimental conditions have been established, the rate constants and the apparent activation energies may be regarded as a significant data depending upon the kinetic parameters.
3) As an application of 2/3 order kinetics, several ilmenite ores have been investigated by means of X ray and X ray microanalyser in addition to the thermogravimetric analysis. It has been found that the reduction process consists of two stages which are as follows:

first stage $Fe_2O_3\ (FeO \cdot TiO_2) \longrightarrow Fe\ (FeO \cdot TiO_2)$
second stage $Fe\ (Fe \cdot TiO_2) \longrightarrow Fe \cdot TiO_2$

The apparent activation energy on the first and second stage was ~20 kcal/mol. ~and ~28 kcal/mol. ~ respectively and these are larger than that in the reduction of iron oxides. From the above-mentioned facts, it may be assumed that the iron oxide in ilmentie ore is associated physically or chemically with the titanium oxide.

References

1) G. Paravano; J. Amer. Chem. Soc., **74**, 1194 (1952).
2) R.E. Cech; Tr. Met. Soc. A.I.M.E., **215**, 759 (1959).
3) J. Bandrowshi, C.R. Bickling, K.H. Yang and O.A. Haugen; Chem. Eng. Sci., **17**, 379 (1962).
4) B. Delmon; Bull. Chim. Soc. France, 590 (1961).
5) T. Imoto and A. Moriyama; Kogyo Kagaku Zasshi, **66**, 297 (1963).
6) W.D. Bond; J. Phys. Chem., **66**, 1563 (1962).
7) K. Mampel; Z. Phys. Chem., A 187, 235 (1940).
8) B. Delmon; Rev. Instit. France du Petrol, **18**, 471 (1963).
9) W.M. McKewan; Tr. Met. Soc. A.I.M.E., **218**, 2 (1960).
10) A. Yamaguchi, M. Takeda and J. Moriyama; J. Min. Met. Inst. Japan, **81**, 93 (1965).
11) H.T.S. Brotton, S.J. Gregg and G.W. Winsor; Trans. Farad. Soc., **48**, 62 (1952).
12) R.P. Marcellini et S.J. Teichner; J. Chim. Phys., **58**, 625, 636 (1961).
13) A. Yamaguchi and J. Moriyama; J. Japan Inst. Metal., **28**, 692 (1964), **29**, 831 (1965).
14) B. Delmon; Rev. Inst. France du Petrole, **16**, 583 (1961).
15) M.T. Simnad; J. Appl. Phys., **29**, 1630 (1958).
16) M.K. Hussein; Z. Erzmetall, **17**. 193 (1964).
17) K. Hedden u. G. Lehman; Arch. Eisenhutten w., **34**, 577 (1963).
18) A. Yamaguchi, M. Takeda and J. Moriyama; Suiyokwai-shi, **15**, 355 (1965) Departments of Mining and Metallurgy, Kyoto University-Japan.